CHINESE OPTICS LETTERS

Vol. 22, No. 2 | February 2024

Towards a fast and stable tachypnea monitor: a C_{60}-Lys enabled optical fiber sensor for humidity tracking in breath progress

Fuxiang Wang (王富祥)[1], Feng Gao (高 峰)[1*], Xiaoniu Wang (王小牛)[1], Ying Wang (王 莹)[2], Fei Jin (金 飞)[2**], Ziqiao Ren (任紫峭)[1], Jun Wu (武 俊)[1], Zhenlin Huang (黄振林)[1], Wenjun Zhou (周文俊)[1], and Changyu Shen (沈常宇)[1***]

[1] College of Optical and Electronic Technology, China Jiliang University, Hangzhou 310018, China

[2] College of Materials and Chemistry, China Jiliang University, Hangzhou 310018, China

*Corresponding author: gaofeng@cjlu.edu.cn

**Corresponding author: jinfei@cjlu.edu.cn

***Corresponding author: shenchangyu@cjlu.edu.cn

Received August 11, 2023 | Accepted September 28, 2023 | Posted Online February 23, 2024

The pandemic of respiratory diseases enlightened people that monitoring respiration has promising prospects in averting many fatalities by tracking the development of diseases. However, the response speed of current optical fiber sensors is still insufficient to meet the requirements of high-frequency respiratory detection during respiratory failure. Here, a scheme for a fast and stable tachypnea monitor is proposed utilizing a water-soluble C_{60}-Lys ion compound as functional material for the tracking of humidity change in the progression of breath. The polarization of C_{60}-Lys can be tuned by the ambient relative humidity change, and an apparent refractive index alteration can be detected due to the small size effect. In our experiments, C_{60}-Lys is conformally and uniformly deposited on the surface of a tilted fiber Bragg grating (TFBG) to fabricate an ultra-fast-response, high-sensitivity, and long-term stable optical fiber humidity sensor. A relative humidity (RH) detecting sensitivity of 0.080 dB/% RH and the equilibrium response time and recovery time of 1.85 s and 1.58 s are observed, respectively. Also, a linear relation is detected between the resonance intensity of the TFBG and the environment RH. In a practical breath monitoring experiment, the instantaneous response time and recovery time are measured as 40 ms and 41 ms, respectively, during a 1.5 Hz fast breath process. Furthermore, an excellent time stability and high repeatability are exhibited in experiments conducted over a range of 7 days.

Keywords: humidity sensor; fullerene derivative; optical fiber sensing; tilted fiber Bragg grating; nanomaterials.
DOI: 10.3788/COL202422.021201

1. Introduction

The human society has been afflicted periodically by the pandemic of respiratory diseases, inflicting huge losses in health, life, and economy. The recent COVID-19 pandemic enlightened people that monitoring the respiratory process and intervening in treatment promptly can avert many fatalities from occurring[1]. It is an investigation focus that combines sensors with breathing equipment and monitoring respiratory status[2]. However, sensors are required to have extremely fast responses and recovery times considering the rapid breath of patients with respiratory failure, which is a formidable challenge. Contrasted with the widely investigated and employed resistance detectors, the optical fiber sensors measure the effective refractive index variation correlated with the intramolecular polarization of functional materials, which circumvents the involvement of electron transfer and transport. Consequently, optical sensors are immune to the capacitance and impedance of the operative circuit and have more merits in devising rapid response relative humidity (RH) sensing elements.

The performance of fiber optic sensors is affected by two factors: fiber structure and functional materials. Generally, the purpose of designing optical structures is to enhance the coupling between light fields and functional materials, thereby encoding the changes of environmental parameters into the optical signals transmitted within optical fiber. As a result, various fiber manufacturing methods, including fiber tapering[3], laser etching[4], side-polishing[5], and microstructure drawing[6], were employed to fabricate optical structures aimed at leaking the optical power

inside the fiber core into cladding. In contrast to the above structures, gratings encompassing a fiber Bragg grating (FBG)[7], long-period fiber grating (LPG)[8], and tilted fiber Bragg grating (TFBG)[9,10] are ultrasensitive and exhibit superior capacities in terms of loss, robustness, practical fabrication attributes, and consistency. Also, considering the environmental disruption, the TFBG proves to be a preferable choice because the core mode in the spectrum is unaffected by the change of refractive index outside fiber and can offset the influences of strain, temperature, and bending, which is important to the RH sensors[11,12].

On the other hand, the selection of functional materials entails equilibrating the adsorption capacity with water molecules, the ability for the conformal deposition on fiber, and the rate of water molecule adsorption and desorption in order to achieve high-performance fiber humidity sensors. Despite the application of the elliptic PMF fabricated TFBG in breath monitoring, which exhibited response and recovery times of 35 ms and 41 ms, respectively, the effectiveness of this method for respiration measurements remains speculative due to its low signal response[13]. The utilization of functional materials in the fabrication of optical humidity sensors continues to be the prevailing approach in contemporary research. At present, sensors have been developed by employing organic materials containing hydrophilic groups, such as polymers[14], sugars[15], and proteins[16], as well as traditional gas sensitive metallic oxides, such as ZnO[17], SnO_2[18], and SiO_2[19]. However, these materials exhibit low-refractive-index changes after adsorbing water molecules and require thick films to achieve a sufficient optical signal response. Consequently, most of these sensors have response times longer than 10 s. Moreover, graphene oxide (GO), as a derivative of 2D material graphene, is drawing extensive research in high-performance fiber RH sensors owing to the small size effect, high surface-area-to-volume ratio, and abundant hydrophilic groups[20-22]. The best performances of a GO enabled fiber humidity sensor were 45 ms and 115 ms in response and recovery progress, respectively[11]. However, the challenge of accurately adhering 2D graphene onto the curved surface of an optical fiber hinders the device's reliability and stability, rendering its consistent performance uncertain. As an allotrope of graphene, C_{60} can be considered as a curved graphene sheet with all dimensions less than 1.0 nm. Compared to graphene, C_{60} derivatives have a stronger small size effect. In our previous work, a fullerene derivative was synthesized by bridging trimethyl aminomethane (Tris) on the C_{60} molecule to increase the hydrophilicity[23]. Then a fiber RH sensor enabled by C_{60}-Tris was developed, and the equilibrium response and recovery times were reported as 2.2 s and 3.2 s, which are still sluggish for breath monitors.

For practical tachypnea monitor application, a rapid response time, data consistency, and temporal stability are indispensable characteristics for sensors. In this paper, a novel methodology is proposed involving solubilizing low-dimensional material fullerene in the fabrication of optical fiber sensors. The affinity of fullerene derivatives for water molecules was enhanced by introducing lysine on the C_{60} surface to prepare C_{60}-Lys. Then the sodium ion salt of C_{60}-Lys was coated on the surface of a TFBG conformally with a nanometric thickness of 480 nm. The substantial variation in refractive index and compact C_{60}-Lys film endows the prepared optical fiber humidity sensor with enhanced sensitivity, high stability, and rapid adsorption–desorption dynamics. Therefore, the sensitivity of 0.080 dB/% RH and equilibrium response and recovery times of 1.85 s and 1.58 s are obtained, respectively. In the respiratory monitor experiment, the instantaneous response and recovery times are measured as 40 ms and 41 ms, respectively. Additionally, a good data consistency and long-term stability are also demonstrated in the experiment.

2. Experimental Section

2.1. Synthesis of fullerene derivatives

In this experiment, a one-step method is employed to prepare the C_{60}-Lys[24]. At first, 100 mL ethanol aqueous solution of 50% concentration was prepared, and then 5.09 g L-lysine and 1.55 g NaOH were dissolved in the solution. After that, 100 mg fullerene was dissolved in 100 mL o-xylene to prepare C_{60} solution. Moreover, a water bath method was taken to keep the lysine solution at 40°C constant; then the fullerene solution was added dropwise to the lysine solution. After stirring for 3 h, the lower layer of the solution was retained. At last, the solvent was evaporated, and then the product was dried at 45°C to get C_{60}-Lys powder.

2.2. Fabrication of C_{60}-Lys enabled TFBG

The TFBG was fabricated by the phase mask method. At first, the excimer laser generated a high-energy pulsed UV laser, and then the light transmitted through a tilted phase mask to a hydrogen-loaded photosensitive fiber. Then a permanent periodic refractive index modulation was written point by point in this progress. In the experiment, the mask period is 542 nm, the length of TFBG L is 15 mm, and the tilt angle θ is 8°. Subsequently, the remaining hydrogen in the fiber was released from the TFBG by a 12 h annealing process at 120°C in a temperature chamber. Finally, the TFBG was immersed in an aqueous C_{60}-Lys solution for 10 min and dried for 20 min at 50°C. We repeated this coating progress until the thin layer of C_{60}-Lys was deposited on the TFBG.

2.3. Working principle of the TFBG enabled fiber humidity sensor

A possible working mechanism of C_{60}-Lys film is proposed and demonstrated in Fig. 1(a). The electronic polarization center of fullerene molecules is located at the center of the spherical carbon cage. However, when small molecules are grafted onto the cage, the polarization center shifts away from the center. Moreover, when water molecules are adsorbed by the grafted molecules, the electronic redistribution alters the polarization center of the fullerene derivative system again, leading to a variation in the polarization intensity. This affects the dielectric

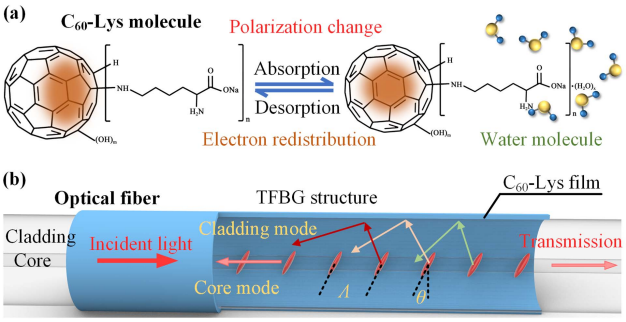

Fig. 1. (a) Working mechanism of C_{60}-Lys film. When water molecules are adsorbed by C_{60}-Lys, the polarization intensity changes. (b) Configuration of the optical fiber humidity sensor. The transmission spectrum is affected by the polarity of C_{60}-Lys.

constant of the fullerene derivative film at a macroscopic level[3]. Meanwhile, the change in dielectric constant is more pronounced for fullerene derivatives due to the size effect[25,26]. Consequently, in practical measurements, there is a significant change in refractive index after water molecule adsorption, and vice versa with desorption.

The optical fiber humidity sensor configuration is illustrated in Fig. 1(b). The C_{60}-Lys layer is deposited on the surface of the TFBG, and the spectrum of the transmission light is employed for the detection of ambient humidity. The working principle of TFBG is discussed in this work. The Bragg mode wavelength λ_{Bragg} and the ith cladding mode resonance wavelength $\lambda^{i}_{\text{cladding}}$ in the TFBG transmission spectrum can be expressed as[27,28]

$$\lambda_{\text{Bragg}} = 2N_{\text{eff}}^{\text{core, Bragg}}\Lambda/\cos\theta, \tag{1}$$

$$\lambda^{i}_{\text{cladding}} = (N_{\text{eff}}^{\text{core},\,i} + N_{\text{eff}}^{\text{cladding},\,i})\Lambda/\cos\theta. \tag{2}$$

In the equation, $N_{\text{eff}}^{\text{core, Bragg}}$ is the effective refractive index of the core mode at the wavelength λ_{Bragg}, $N_{\text{eff}}^{\text{core},\,i}$ is the effective refractive index of the core mode, $N_{\text{eff}}^{\text{cladding},\,i}$ is the cladding mode at the wavelength $\lambda^{i}_{\text{cladding}}$, Λ is the interference pattern period of the TFBG mask, and θ is the inclination angle of the grating plane relative to the cross-section plane of the fiber. The resonance intensity of the TFBG, also known as power reflectivity R, is related to the coupling coefficient κ between the incident core mode and the phase matching mode and the length L of the grating. It can be expressed as follows:

$$R = \tanh^2(\kappa L). \tag{3}$$

The coupling coefficient κ is calculated as follows:

$$\kappa = C\iint \vec{E}^{*}_{\text{core}} \cdot \vec{E}_r \Delta n(x,y)\mathrm{d}x\mathrm{d}y, \tag{4}$$

where C is the proportional constant related to the normalization of the transverse mode fields (E_{core} and E_r), and $\Delta n(x,y)$ is the function describing the refractive index perturbation caused by gratings in the fiber cross section. In this work, the change of refractive index of C_{60}-Lys film is the reason for the perturbation of $\Delta n(x,y)$. The refractive index of C_{60}-Lys increases gradually, which will result in a gradual decrease in the resonance intensity of the TFBG cladding mode.

2.4. Experiment setup

The experimental setup of the proposed TFBG humidity sensor is depicted in Fig. S1 (Supplementary Material). In the experiment, a broadband light source (BBS, Hoyatek) with a wavelength range of 1420–1620 nm was used as the input light. The polarization state of the light was adjusted to the P state by a polarization controller (PC, PR2000, JDS Uniphase). Moreover, the spectrometer (OSA, AQ6370D, Yokogawa) with a wavelength resolution of 0.05 nm was applied to record the output spectrum. Humidity atmosphere was generated in a chamber by adjusting the ratio of dry or moist. A hygrometer (Jiandarenke, tolerance 1.5% RH) was applied for the detection of accurate RH data. At last, the fiber humidity sensor was fixed in the chamber and the RH change can be observed from the spectrum recorded by the OSA. Since RH is a physical parameter associated with temperature, all the experiment in this work was conducted at room temperature controlled by an air conditioner.

3. Results and Discussion

3.1. Characterization of C_{60}-Lys film

Fourier transform infrared spectroscopy (FTIR) analysis was conducted for the synthetic product. As shown in Fig. 2(a), the broad absorption peak at 3412.4 cm^{-1} corresponds to N-H or O-H bonds, while the absorption peak at 1462.3 cm^{-1} (C-C) represents the characteristic peak of C_{60}. Vibrations of C-H, C=O, and C-N bonds are observed at 2918.3, 1582.3, and 1115.1 cm^{-1}, respectively.

The carrier density of C_{60} is biased at a high concentration due to the small size; therefore, the RI change can be easily observed if the polarization is altered by the gas absorption. The strong hydrophilicity and simple synthesis method of lysine enabled the success of the experiment.

In this work, a scanning electron microscope (SEM) was used to characterize the film deposition results of C_{60}-Lys on optical fiber. As shown in Fig. 2(b), the side view indicates that the film coated on the optical fiber is overall uniform. The inset is the energy dispersive spectrum (EDS), in which C is the elements in the C_{60}-Lys, Si and O come from the silica fiber, and Al is element of the metal stage used for the placing of optical fiber. Moreover, the thickness of the C_{60}-Lys film is observed as 480 nm in the profile image in Fig. 2(c). The uniform and compact C_{60}-Lys layer along the fiber surface illustrated in the SEM images facilitates the rapid adsorption–desorption dynamics.

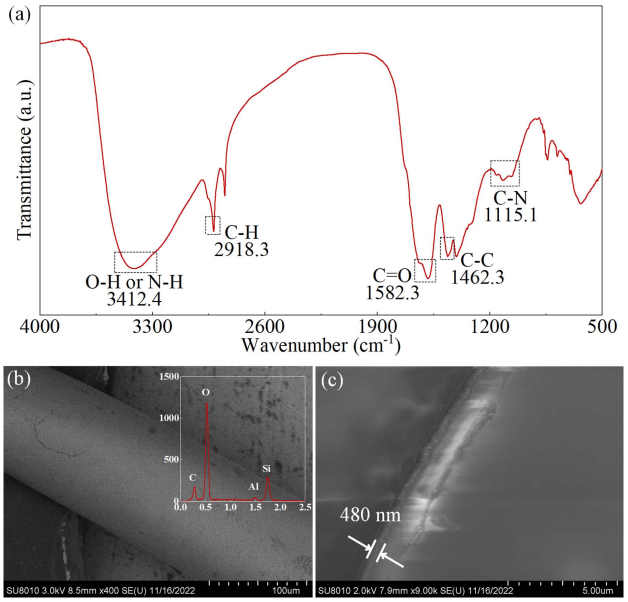

Fig. 2. (a) FTIR spectrum of C_{60}-Lys. (b) SEM image of the surface of TFBG. The inset is the dispersive energy spectrum (EDS) of the TFBG surface, which is evidence for the existence of C_{60}-Lys film on fiber. (c) Cutting face SEM image of the C_{60}-Lys film.

3.2. RH detection with FHS

The spectrum response of the fiber humidity sensor (FHS) was researched in this work. The experiment results are illustrated in Fig. 3. The spectrum recorded by OSA was a typical transmission spectrum of TFBG, as shown in Fig. 3(a). The period of high-order-mode resonance is about 1.35 nm, and the max extinction ratio is observed around 1518 nm. The inset is the enlarged figure of core mode resonance around 1583.23 nm. The wavelength sensitivity of the core mode is about 0.078 pm/% RH. The results indicate that the core mode of the TFBG is humidity insensitive to the RH change, and it can be used to compensate for the temperature. In the experiment, the RH was increased from 30% to 90% with an increment of 10%. When the RH of the environment was varied, the resonance strength of high-order mode was altered, and the reflection intensity can be employed for measuring the RH. In this work, the resonance strength around 1518 nm was selected for the RH detection, as illustrated in Fig. 3(b). As the RH increased from 40% to 80%, the intensity of cladding mode changed from −17.542 dB to −12.537 dB. A slight red shift of the wavelength was also observed from the spectrum. The total wavelength shift was about 33 pm as the RH changed from 30% to 90%.

Experiment results indicate that the FHS in this work is a linear response device as shown in Fig. 3(c). The intensity versus relative humidity is plotted in blue color. A linear fit is conducted, and the sensitivity of the device is calculated as 0.080 dB/% RH with a linear correlation coefficient of 0.9577. Moreover, the humidity induced wavelength shift is plotted by the red color. The wavelength sensitivity is about 0.55 pm/% RH. In the context of humidity sensing, this level of response is

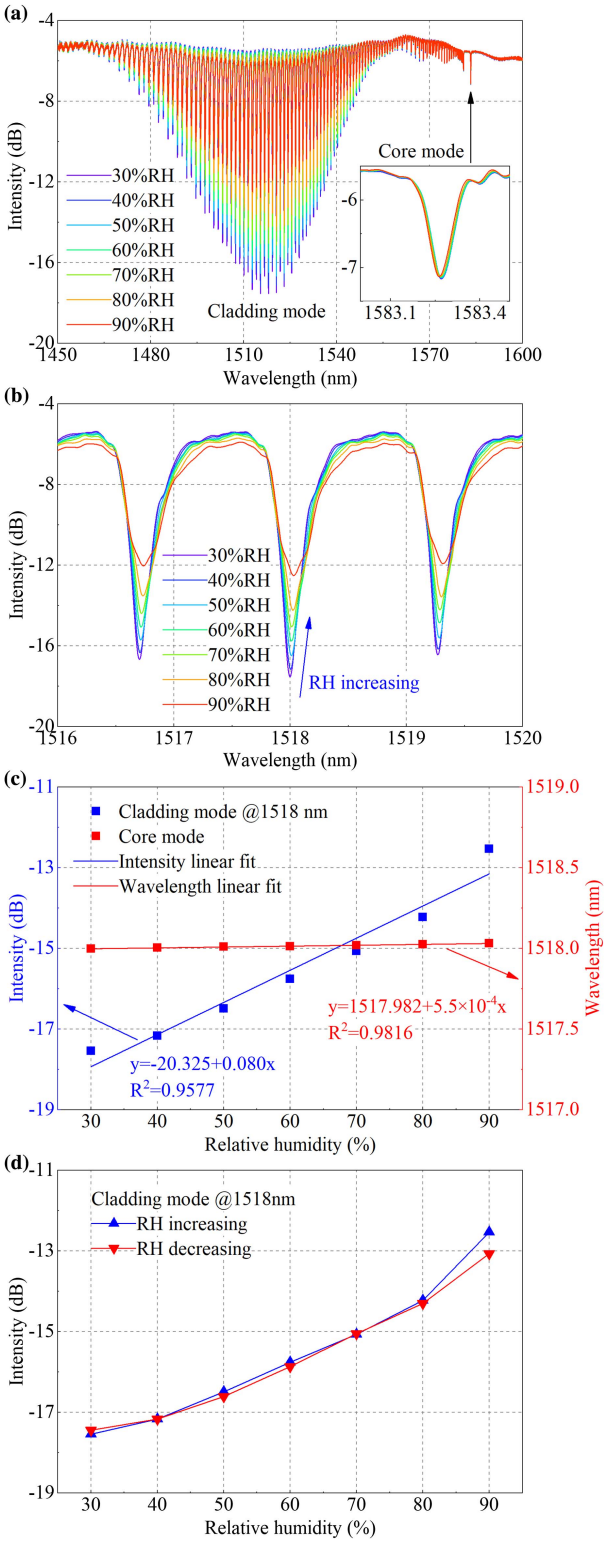

Fig. 3. (a) RH detection results by the FHS. The transmission spectra of FHS at the environment RH raising from 30% to 90% with the inset showing changes at the core mode. (b) Detailed variation of the cladding mode in the wavelength range from 1516 nm to 1520 nm. (c) The blue line is the linear fitting of intensity and RH at the cladding mode of 1518 nm. The red line is the linear fitting of wavelength and RH at the cladding mode of 1518 nm. (d) Comparison of cladding mode intensities at 1518 nm with increasing and decreasing RH.

negligible and can be disregarded. A reversal experiment was taken to analyze the recovery performance of the FHS. As shown in Fig. 3(d), the spectrum returned to its original state as the humidity reduced from 90% to 30% with an increment of 10%. The results reveal that the FHS enabled by C_{60}-Lys is reversible, and the devices exhibit a low humidity hysteresis. Furthermore, the decrease in the resonance intensity of the TFBG cladding mode illustrates that the refractive index of the C_{60}-Lys film is increased.

3.3. Equilibrium response time

The equilibrium response time of gas sensors is an important parameter. However, the measurement of equilibrium response time for a fast response FHS is difficult since a rapid change of environmental humidity needs to be achieved, and the humidity should keep stable for a period of time. We improved the device in Fig. S1 (Supplementary Material) to obtain a fast change of humidity atmosphere by reducing the volume of the gas chamber. The detailed experiment setup is illustrated in Fig. 4(a). The initial gas with humidity concentration of 80% was put in a chamber. Then a pump with two outputs was placed in the chamber, and it was applied as a gas pressure source. A valve was installed at one path of the air and another path transmitted through a conical flask filled with desiccant. The two air paths were connected by a Y-tube. A small volume narrow tube was employed as a gas chamber, and an optical sensor was placed in it. The air from the Y-tube was injected in the narrow chamber. Moreover, the tail gas was collected by a small chamber, and the humidity was detected by a resistance hygrometer.

In the experiment, the wavelength of the OSA was settled at 1518 nm, and the scanning point amount was set as 1001. Then the time resolution was calculated as 0.045 s between each adjacent point. In this case, the intensity change of the cladding mode at 1518 nm versus time can be plotted by the scanning data from OSA. Experimental results correlating with the ambient humidity fluctuation from 40% to 45% are demonstrated in Fig. 4(b), whereas data pertaining to a humidity change in the range of 60% to 80% are presented in Fig. 4(c). The time interval for the change of valve state was about 5 s. Four periods were recorded, and the performance of humidity sensors in each cycle shows strong consistency. However, the pressure of the gas will change as the valve state is altered. As a result, the response figure shows little disturbance at each time when opening or closing the valve.

The enlarged picture of one period is illustrated in Fig. 4(c) for the calculation of reaction time. The absorption and desorption processes demonstrate a decaying-exponential response until the surface coverage of the absorbing material reaches saturation[29]. In this work, the T90 rule, which refers to the time a sensor takes to reach 90% of its final state value after a step change in input, was applied to calculate the response time. As shown in Fig. 4(b), the response time and recovery time are calculated as 1.85 s and 1.58 s in the T90 rule when the humidity changes between 40% and 45%, respectively. The response and recovery times are calculated as 5.52 s and 2.52 s as the humidity

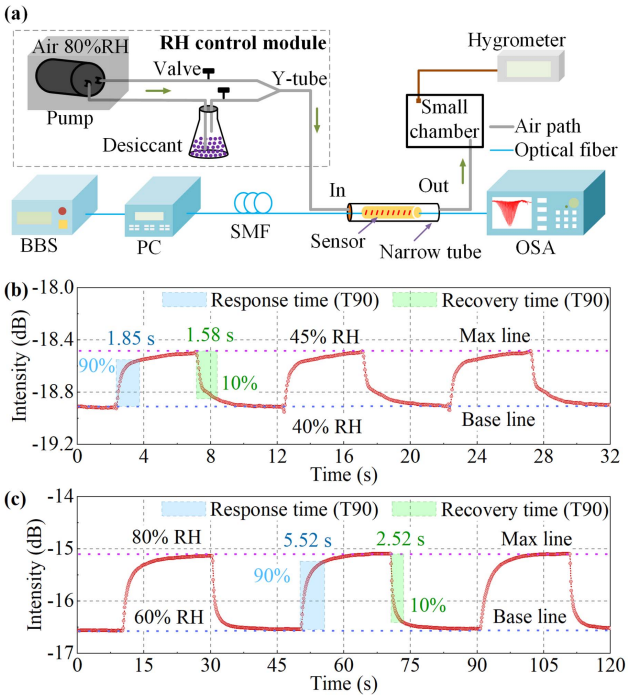

Fig. 4. (a) Experimental setup of response time. Controlling the opening of the valve to change the air RH. (b) Results of change between 40% RH and 45% RH, and the response time and recovery time are calculated as 1.85 s and 1.58 s, respectively. (c) Results of change between 60% RH and 80% RH. The performance of the sensor is ultra-stable.

changes from 60% to 80% in Fig. 4(c). The equilibrium time performance of recent humidity sensors based on optical fiber is summarized and listed in Table S1 (Supplementary Material).

3.4. Breath monitoring experiment

The proposed FHS in this work was integrated with a breathing tube and then applied for breath monitoring. The optical path is shown in Fig. 5(a). A volunteer was instructed to employ various respiratory rates, simulating tachypnea, to examine the reaction of the FHS. The details of the breathing tube are shown in Fig. 5(b). Firstly, one end of the silica fiber was inserted from outside into the breathing tube. Secondly, the fiber was exited and a 20 mm length fiber was left inside the breathing tube. After that, the optical fiber was secured by UV light curing adhesives to ensure that 15 mm long TFBG was exactly placed inside the breathing tube. The experiment results are illustrated in Fig. 5. In the experiment, the time scan interval of the OSA was set to 0.009 s, and the total time of the measurement was about 9 s. The data collected by the OSA are plotted in Figs. 5(c), 5(d), and 5(e), corresponding to the three tachypnea experiments, respectively. The response and recovery times of the FHS are calculated from the enlarged figure shown in Figs. 6(f), 6(g), and 6(h). The response time and recovery time are calculated as 45 ms and 126 ms, respectively, in Test-1, 44 ms and 81 ms in Test-2, and 40 ms and 61 ms in Test-3 with the T90 rule. What is noteworthy is that the intensity change between the breath on

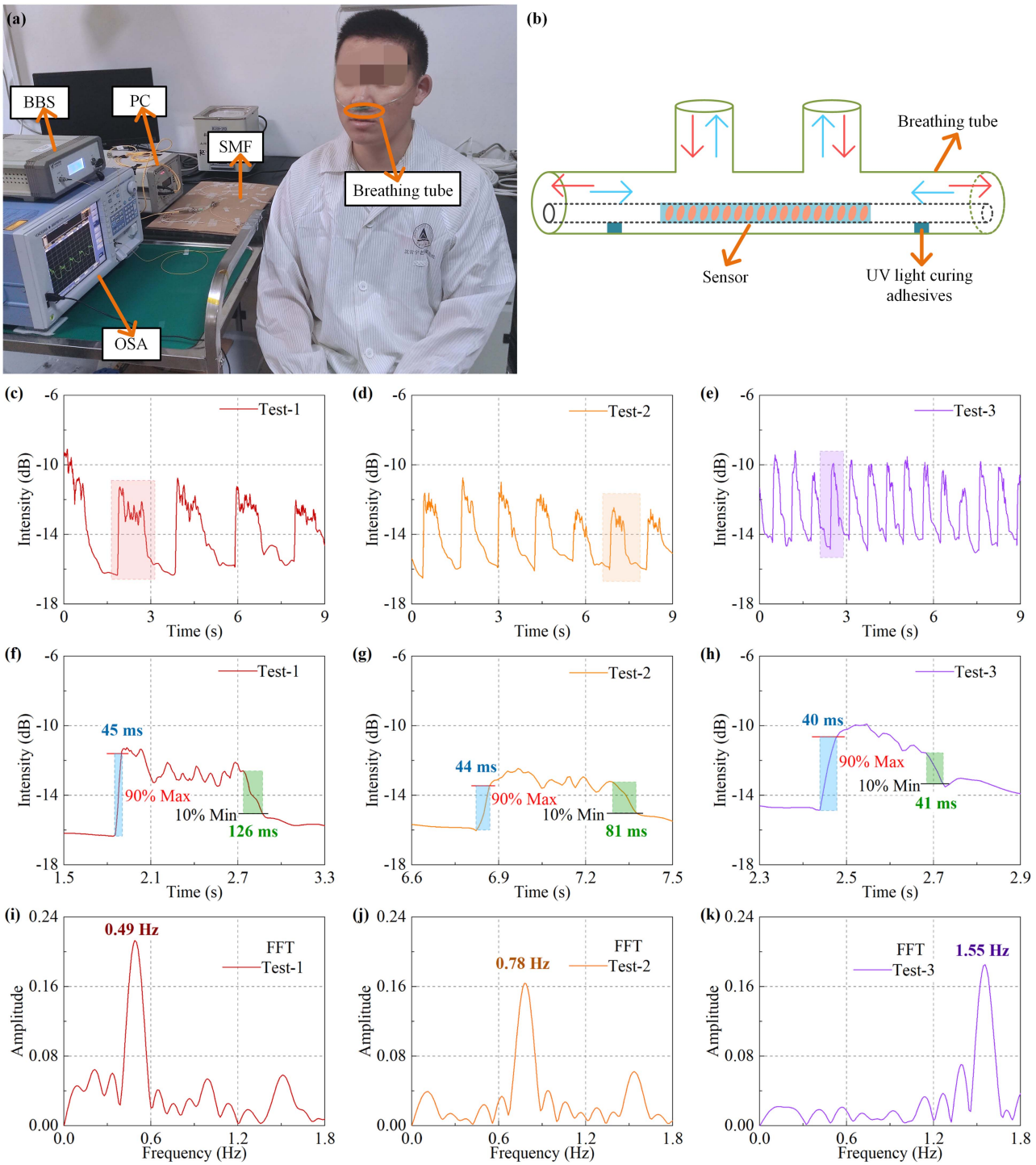

Fig. 5. Results of breath monitoring experiments. (a) Breath monitoring optical path. (b) Combination of the sensor and breathing tube. (c)–(e) Spectra at Test-1, Test-2, and Test-3 with different respiratory frequencies. (f)–(h) Response times of one breath at three tests. (i)–(k) FFT calculates the frequency of three tests.

and off was about 4 dB in the detection progress. The results indicate the fast respiration can be properly detected, and the FHS was working in a normal frequency bandwidth. Fourier transforms were taken, and the results are exhibited in Figs. 6(i), 6(j), and 6(k); the frequency is calculated as 0.49 Hz, 0.78 Hz, and 1.55 Hz corresponding to the three tachypnea experiments.

The response and recovery times detected from the breath monitor experiments are concluded and illustrated in Table S2 (Supplementary Material) and Fig. 6. The C_{60}-Lys fiber sensor proposed in this study demonstrates a sustained level of excellence in response time performance for respiration monitoring. Compared to the elliptic PMF fabricated TFBG (E-HIPFG),

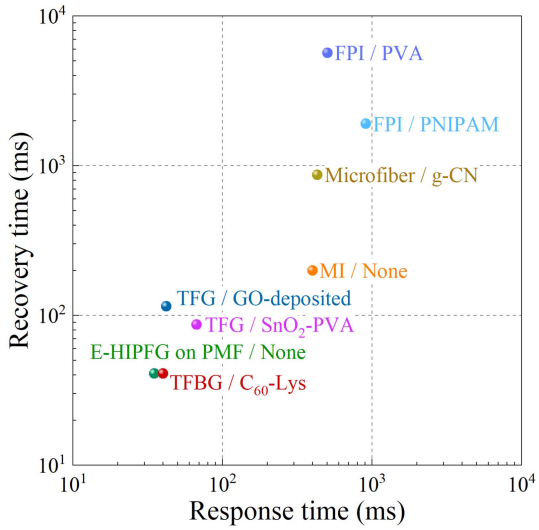

Fig. 6. Comparison of the response time and recovery time of our FHS with different materials coated with optical fiber sensor.

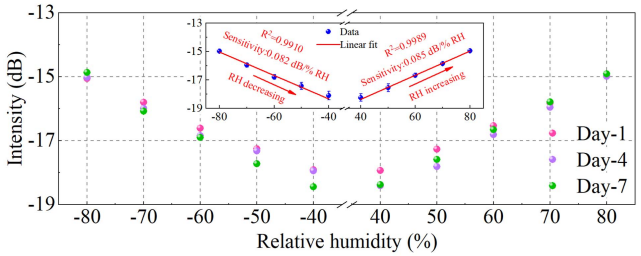

Fig. 7. Stability test results of FHS within 7 days. The inset figure is the linear fit results.

the intensity sensitivity of humidity measured in this work has an advantage about one order of magnitude.

3.5. Temporal stability of the FHS

The temporal stability of the FHS is essential for its practical application, which depends on the durability of functional material and the reliability of the functional optical structure. In this work, the temporal performance of the C_{60}-Lys enabled TFBG was researched by an experiment lasting 7 days. The results are illustrated in Fig. 7. As the ambient humidity changed from 40% to 80%, the humidity responses at Day-1, Day-4, and Day-7 were recorded and they are plotted in pink, purple, and green, respectively. The inset figure is the linear fit results. The sensitivity in the RH decreasing process is about 0.082 dB/% RH and about 0.085 dB/% RH in the rising process. The sensitivity change is about 3.5% between the rising and decreasing progress. Our device proposed in this work has a strong linear response, repeatability, and long-term stability.

4. Conclusion

In conclusion, a C_{60}-Lys enabled fiber optic sensor is proposed for the tracking of humidity change in breath progress. The sensor is a promising candidate for fast and stable tachypnea monitoring considering the characteristics of ultra-fast response, high data consistency, and good time stability demonstrated in experiment. The uniform deposition of C_{60}-Lys on the TFBG surface was confirmed by SEM and EDS. The change in refractive index of the C_{60}-Lys film has a significant impact on the resonance intensity of the cladding mode of the TFBG in different humidity environments. The experimental results show that the sensitivity is 0.080 dB/% RH with a high linear coefficient in the range of 40%–80% RH. In the human respiration monitoring experiment, the instantaneous response time and recovery time are about 40 ms and 41 ms, respectively. In addition, the method of preparing high-stability optical fiber sensors by solubilizing low-dimensional material fullerene to facilitate the coating quality was proposed in this work. This method is beneficial to the development of new optical fiber functional devices.

Acknowledgements

This work was supported by the National Natural Science Foundation of China (Nos. 12274386 and 52002365), Zhejiang Provincial Natural Science Foundation of China (Nos. LQ23F050006, LY21F050006, and LQ21E020005), Key R & D Project of Zhejiang Province (No. 2021C01179), and National Key R & D Program of China (No. 2021YFF0600203).

References

1. F. Collins, S. Adam, C. Colvis, *et al.*, "The NIH-led research response to COVID-19: investment, collaboration, and coordination have been key," Science **379**, 441 (2023).
2. X. Xue, X. Han, L. Li, *et al.*, "Real-time monitoring of human breathing using wearable tilted fiber grating curvature sensors," J. Lightwave Technol. **41**, 4531 (2022).
3. Q. Chen, F. Gao, D. N. Wang, *et al.*, "Electrically tunable optical filter based on tapered fiber coated with porous graphene film," Opt. Commun. **505**, 5 (2022).
4. M. Q. Chen, T. Y. He, and Y. Zhao, "Review of femtosecond laser machining technologies for optical fiber microstructures fabrication," Opt. Laser Technol. **147**, 16 (2022).
5. R. Chu, C. Y. Guan, Y. T. Bo, *et al.*, "All-optical graphene-oxide humidity sensor based on a side-polished symmetrical twin-core fiber Michelson interferometer," Sens. Actuators B Chem. **284**, 623 (2019).
6. J. Kapit and A. P. M. Michel, "Dissolved gas sensing using an anti-resonant hollow core optical fiber," Appl. Opt. **60**, 10354 (2021).
7. M. Tian, Y. H. Huang, C. Li, *et al.*, "High-performance humidity sensor based on a micro-nano fiber Bragg grating coated with graphene oxide," Opt. Express **28**, 26395 (2020).
8. F. Esposito, L. Sansone, A. Srivastava, *et al.*, "Long period grating in double cladding fiber coated with graphene oxide as high-performance optical platform for biosensing," Biosens. Bioelectron. **172**, 112747 (2021).
9. M. Lobry, M. Loyez, M. Debliquy, *et al.*, "Electro-plasmonic-assisted biosensing of proteins and cells at the surface of optical fiber," Biosens. Bioelectron. **220**, 114867 (2023).
10. C. Y. Shen, D. J. Liu, X. K. Lian, *et al.*, "Microfluidic flow direction and rate vector sensor based on a partially gold-coated TFBG," Opt. Lett. **45**, 2776 (2020).
11. B. Q. Jiang, Z. X. Bi, Z. Hao, *et al.*, "Graphene oxide-deposited tilted fiber grating for ultrafast humidity sensing and human breath monitoring," Sens. Actuators B Chem. **293**, 336 (2019).

12. C. Y. Shen, C. Zhong, D. J. Liu, *et al.*, "Measurements of milli-Newton surface tension forces with tilted fiber Bragg gratings," Opt. Lett. **43**, 255 (2018).
13. L. T. Hou, Y. Li, Y. M. Fu, *et al.*, "Ultra-sensitive optical fiber humidity sensor via Au-film-assisted polyvinyl alcohol micro-cavity and Vernier effect," IEEE Trans. Instrum. Meas. **71**, 7002009 (2022).
14. C. G. Yu, H. P. Gong, Z. X. Zhang, *et al.*, "Optical fiber humidity sensor based on the Vernier effect of the Fabry-Perot interferometer coated with PVA," Opt. Fiber Technol. **67**, 7 (2021).
15. A. M. Shrivastav, D. S. Gunawardena, Z. Y. Liu, *et al.*, "Microstructured optical fiber based Fabry-Perot interferometer as a humidity sensor utilizing chitosan polymeric matrix for breath monitoring," Sci. Rep. **10**, 10 (2020).
16. Y. T. Yi, Y. X. Jiang, H. Y. Zhao, *et al.*, "High-performance ultrafast humidity sensor based on microknot resonator-assisted Mach-Zehnder for monitoring human breath," ACS Sens. **5**, 3404 (2020).
17. S. Azad, E. Sadeghi, R. Parvizi, *et al.*, "Fast response relative humidity clad-modified multimode optical fiber sensor with hydrothermally dimension controlled ZnO nanorods," Mater. Sci. Semicond. Process. **66**, 200 (2017).
18. N. A. Siddiq, W. Y. Chong, Y. H. Pramono, *et al.*, "All-optical humidity sensor using SnO_2 nanoparticle drop coated on straight channel optical waveguide," Photonic Sens. **10**, 123 (2020).
19. C. Y. He, S. Korposh, R. Correia, *et al.*, "Optical fibre sensor for simultaneous temperature and relative humidity measurement: towards absolute humidity evaluation," Sens. Actuators B Chem. **344**, 130154 (2021).
20. X. Ding, J. C. Yan, N. Chen, *et al.*, "Highly sensitive balloon-like fiber interferometer based on GO nanomaterial coated for humidity measurement," Opt. Laser Technol. **158**, 108798 (2023).
21. Y. Q. Sun, J. C. Guo, Y. F. Xiao, *et al.*, "Twisted weakly coupled relative humidity sensor coated with a graphene oxide/polyvinyl alcohol composite," Appl. Opt. **61**, 6658 (2022).
22. F. Wang, B. W. Wang, X. H. Zhang, *et al.*, "High sensitivity humidity detection based on functional GO/MWCNTs hybrid nano-materials coated titled fiber Bragg grating," Nanomaterials **11**, 1134 (2021).
23. X. S. Wu, F. Gao, F. Jin, *et al.*, "Optical fiber humidity sensor with C-60-THAM as molecule receptors," Sens. Actuators B Chem. **370**, 132344 (2022).
24. N. A. Charykov, V. A. Keskinov, and A. V. Petrov, "Adducts of lower fullerenes and amino acids: synthesis, identification, and quantum-mechanical modeling of their physicochemical properties," Russ. J. Phys. Chem. A **95**, 2359 (2021).
25. P. Holmstrom, L. Thylen, and A. Bratkovsky, "Dielectric function of quantum dots in the strong confinement regime," J. Appl. Phys. **107**, 064307 (2010).
26. J. M. Luther, P. K. Jain, T. Ewers, *et al.*, "Localized surface plasmon resonances arising from free carriers in doped quantum dots," Nat. Mater. **10**, 361 (2011).
27. J. Albert, L. Y. Shao, and C. Caucheteur, "Tilted fiber Bragg grating sensors," Laser Photonics Rev. **7**, 83 (2013).
28. C. Y. Shen, X. K. Lian, V. Kavungal, *et al.*, "Optical spectral sweep comb liquid flow rate sensor," Opt. Lett. **43**, 751 (2018).
29. D. A. Knopf and M. Ammann, "Technical note: adsorption and desorption equilibria from statistical thermodynamics and rates from transition state theory," Atmos. Chem. Phys. **21**, 15725 (2021).